

Magnetic Materials | Hot Paper |

A Mononuclear Uranium(IV) Single-Molecule Magnet with an Azobenzene Radical Ligand

Maria A. Antunes,^[a] Joana T. Coutinho,^[a] Isabel C. Santos,^[a] Joaquim Marçalo,^[a] Manuel Almeida,^[a] José J. Baldoví,^[b] Laura C. J. Pereira,^{*[a]} Alejandro Gaita-Ariño,^{*[b]} and Eugenio Coronado^{*[b]}

Abstract: A tetravalent uranium compound with a radical azobenzene ligand, namely, $[(\text{SiMe}_2\text{NPh})_3\text{-tacn}]\text{U}^{\text{IV}}(\eta^2\text{-N}_2\text{Ph}_2^*)$ (**2**), was obtained by one-electron reduction of azobenzene by the trivalent uranium compound $[\text{U}^{\text{III}}\{(\text{SiMe}_2\text{NPh})_3\text{-tacn}\}]$ (**1**). Compound **2** was characterized by single-crystal X-ray diffraction and ^1H NMR, IR, and UV/Vis/NIR spectroscopy. The magnetic properties of **2** and precursor **1** were studied by static magnetization and ac susceptibility measurements,

which for the former revealed single-molecule magnet behaviour for the first time in a mononuclear U^{IV} compound, whereas trivalent uranium compound **1** does not exhibit slow relaxation of the magnetization at low temperatures. A first approximation to the magnetic behaviour of these compounds was attempted by combining an effective electrostatic model with a phenomenological approach using the full single-ion Hamiltonian.

Introduction

Driven by new physics and remarkable potential applications in data storage and quantum computing, single-molecule magnets (SMMs) have become an important topic of research.^[1–9] First observed in polynuclear aggregates of paramagnetic transition-metal ions, it was initially believed that high-spin clusters were required to generate such behaviour.^[1,5] However, in 2003 seminal work by Ishikawa and co-workers revealed that bis-phthalocyanine lanthanide(III) compounds containing a single paramagnetic ion, Tb or Dy, exhibited SMM behaviour as well.^[10] Since then, an increasing number of SMMs based on mononuclear lanthanide compounds^[5,11–14] and, more recently, mononuclear actinide^[5,15–18] and transition-metal complexes^[5,19] have been reported. These compounds are generally known as single-ion magnets (SIMs).

In spite of some important advances,^[5,6,12,18,20–25] the SMM phenomenon in these mononuclear complexes is far from being well understood. The development of new SIMs with improved magnetic properties is thus still dependent on a more detailed understanding of the parameters underlying slow magnetic relaxation and its mechanism. In this respect, it is im-

portant to compare related compounds to clearly probe selected effects such as coordination geometry, nature of ligands and crystal-field strength, oxidation state of the metal, as well as the effects of magnetic dilution and magnetic exchange coupling. In this context, the study of actinide-based complexes is considered an emerging topic. In fact, due to the properties of the 5f electrons, actinides exhibit stronger spin-orbit coupling interactions, larger magnetic anisotropy and enhanced exchange interactions. Thus, they can be considered to be better candidates to provide SIMs than lanthanides, as the J ground-state splitting caused by the ligand field is expected to be larger.^[15,18] Although some examples have been reported in the last few years, SIMs based on actinides are still scarce and mainly restricted to U^{III} species; aside from a few distinct compounds,^[16,17,26,27] most studies have focused on poly(pyrazolyl)-borate uranium complexes.^[28–36] These studies on wisely selected compounds could clearly evidence the effects of axial^[27–29,32–34,36] and non-axial ligand environments,^[16,17,27,31,35] magnetic dilution,^[30] charge of the coligand,^[31,35] different ligand donor strength in the same trigonal-prismatic^[34] and tetrahedral^[16] coordination geometries and also the first comparative studies with isostructural lanthanide complexes.^[32,34]

The effect of the oxidation state of uranium, which is known to exist in the range +2 to +6, has remained less explored. U^{VI} is a diamagnetic ion and, at the other extreme, molecular U^{II} species only recently have been isolated in the solid state.^[37,38] In the range +3 to +5, besides the U^{III} complexes mentioned above, only one example based on a mononuclear uranium(V) system has been identified,^[39] and so far no examples of SMMs based on uranium(IV) have been reported. The U^{IV} ion, an f^2 system with a $^3\text{H}_4$ ground state, is a non-Kramers ion that generally exhibits an orbital singlet ground state at low temperatures.^[40] Lacking the magnetic bistability of the ground state

[a] Dr. M. A. Antunes, J. T. Coutinho, Dr. I. C. Santos, Dr. J. Marçalo, Prof. M. Almeida, Dr. L. C. J. Pereira
C²TN, Instituto Superior Técnico, Universidade de Lisboa
Estrada Nacional 10, 2695-066 Bobadela LRS (Portugal)
E-mail: lpereira@ctn.ist.utl.pt

[b] J. J. Baldoví, Dr. A. Gaita-Ariño, Prof. E. Coronado
Instituto de Ciencia Molecular, Universitat de València
C/Catedrático José Beltrán 2, 46980 Paterna (Spain)
E-mail: alejandro.gaita@uv.es
eugenio.coronado@uv.es

Supporting information and ORCID IDs from the authors for this article are available on the WWW under <http://dx.doi.org/10.1002/chem.201503133>.

required for slow magnetic relaxation,^[20] U^{IV} is thus believed not to be a suitable candidate for generating SIMs,^[21] and, in fact, SMM behaviour was explicitly reported as absent in some U^{IV} compounds.^[41–44]

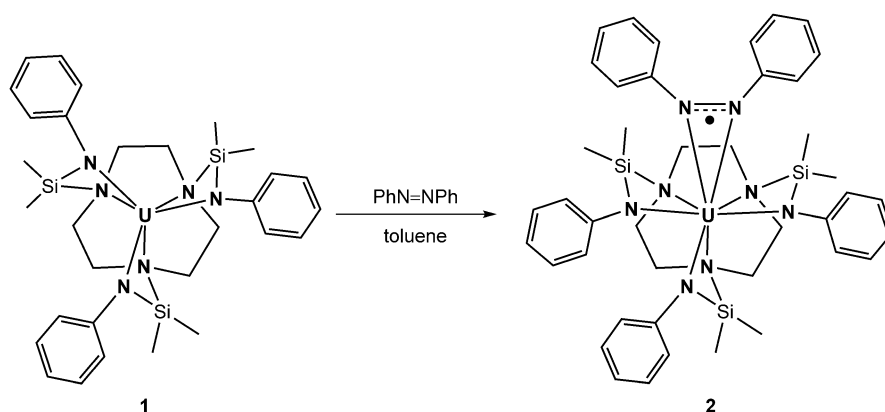
However, an appropriate choice of the coordination environment and the presence of a radical may circumvent this constraint. In fact, coupling of a magnetic ion to an organic radical can have dramatic effects on magnetic relaxation. It has been shown that a radical can slow down quantum tunnelling relaxation pathways.^[13] Indeed, it was recently demonstrated that the presence of a radical ligand in the compound $[U^{III}(Tp^{Me_2})_2(bipy^{\bullet})]$ ($bipy^{\bullet}$ = bipyridine radical) induces the appearance of slow magnetic relaxation in zero static magnetic field.^[35] In the case of lanthanides, seminal work in this context was reported by Evans, Long et al.,^[45,46] who linked two Dy^{III} or two Tb^{III} ions via a $[N_2]^{3-}$ radical, and demonstrated that the resulting system can enhance the exchange coupling between their spins and produce record high blocking temperatures. Nevertheless, while exchange coupling mediated by a radical can block tunnelling when the anisotropy axes of the connected SIMs are parallel, it can enhance tunnelling if they are not.^[47] The effect of the radical in this kind of complex is not limited to enhanced exchange between two metal ions. For a single rare earth metal ion coupled to a radical ligand, dramatic effects are also expected. For example, depending on the symmetry of the system, diagonal or off-diagonal terms will act, blocking or enhancing tunnelling, respectively. Additionally, the presence of an extra electron switches the magnetic system from half to integer spin or vice versa. An illustrative situation is that of a Kramers ion, for example, Er^{III} or U^{III} , for which tunnelling is strictly forbidden when isolated. However, if coupled to a half-integer spin (a radical) its spin is able to flip. In fact, the main effect in this case of the extra electron spin is to switch the parity from Kramers to non-Kramers. Thus, the goal in this work is to apply the same principle to a non-Kramers ion (U^{IV}) to produce a Kramers magnetic molecule capable of slow relaxation of the magnetization.

Herein, we report the magnetic properties of a U^{IV} complex containing an azobenzene radical ligand, namely, $[(SiMe_2NPh)_3-tacn]U^{IV}(\eta^2-N_2Ph_2)$ (**2**). This compound is obtained from a one-electron reduction of azobenzene by the previously described trivalent uranium compound $[U^{III}\{(SiMe_2NPh)_3-tacn\}]$ (**1**).^[48] The magnetic properties of **1** were also studied. In the light of the results reported so far, complex **1** is the first example of a U^{III} compound that does not exhibit slow relaxation of the magnetization. These results are understood within an effective electrostatic model based on the crystal-field theory and the full single-ion Hamiltonian.

Results and Discussion

Synthesis and structural characterization

The synthetic strategy used to prepare the compound $[(SiMe_2NPh)_3-tacn]U^{IV}(\eta^2-N_2Ph_2)$ (**2**), known to exist since 2005,^[49,50] was based on our work with the trivalent uranium complex $[U^{III}\{(SiMe_2NPh)_3-tacn\}]$ (**1**), which engages in one-electron reduction of halogenated and chalcogenide substrates to afford U^{IV} derivatives,^[48,49,51] as well as in two-electron reduction of elemental sulfur leading to the formation of a terminal U^V persulfide.^[51] Thus, the addition of one equivalent of azobenzene to a toluene solution of compound **1** leads, after appropriate workup, to a dark green powder in 59% yield. Characterization by 1H NMR spectroscopy and single-crystal X-ray diffraction proved this product to be a uranium(IV) compound with an azobenzene radical anion, namely, $[(SiMe_2NPh)_3-tacn]U^{IV}(\eta^2-N_2Ph_2)$ (**2**; Scheme 1). Compound **2** was also characterized by IR, UV/Vis/NIR and EPR spectroscopy (see the Supporting Information).



Scheme 1. Synthesis of **2**.

The reduction of azobenzene with formation of a radical anion or even a dianionic ligand has been performed with different lanthanide systems,^[52–60] but it was not previously described in uranium chemistry. Actually, the examples reported in the literature concerning the reaction of uranium compounds with azobenzene have always resulted in reductive cleavage of the $N=N$ bond to form bis(phenylimido) derivatives. These reactions occur by a multi-electron redox process involving the metal centre and the ligands in the case of U^{III} and U^{IV} ^[61–64] or just the metal centre in the case of U^{II} .^[65–68] The absence of a redox-active ligand in the coordination environment of the U^{III} compound **1** favours a single-electron reduction process with the concomitant formation of **2**, as shown in Scheme 1.

Compound **2** crystallizes readily as dark green crystals from common solvents such as THF or toluene; however, single crystals suitable for X-ray diffraction studies could be obtained only from a $[D_6]$ benzene solution of **2** kept at room temperature. This compound crystallizes in the triclinic space group $P\bar{1}$,

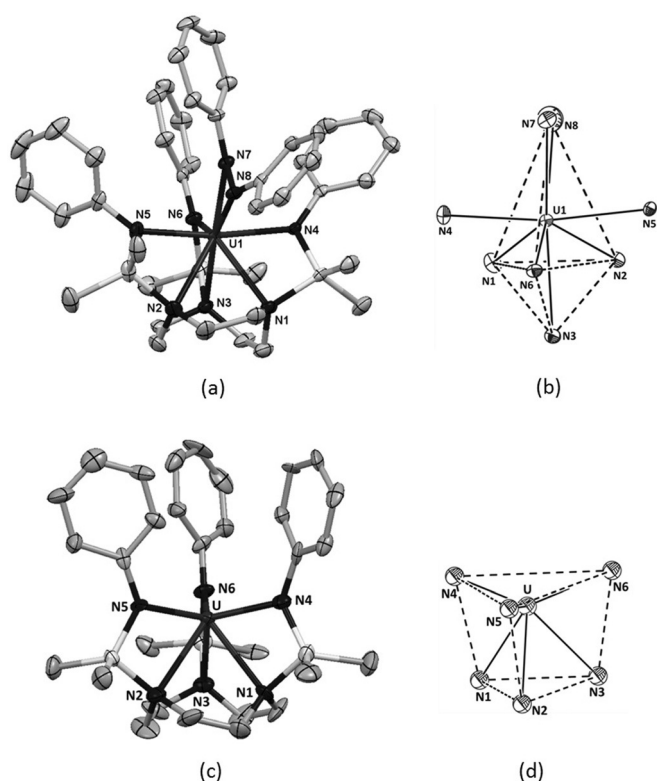


Figure 1. Molecular structures and coordination geometries of **2** (a, b) and **1** (c, d) (thermal ellipsoids set at 40 and 20% probability, respectively; see also Figure S1 of the Supporting Information). Hydrogen atoms, the second independent molecule for **2** and solvent molecule for **1** were omitted for clarity. Bond lengths [Å] for **1**: U–N_{amido} 2.326(19)–2.367(15) Å; U–N_{amine} 2.640(18)–2.677(19) Å.^[48]

with two crystallographically independent molecules in the asymmetric unit. In each molecule, the uranium atom is eight-fold-coordinated by the three nitrogen atoms of the macrocycle, the three nitrogen atoms of the pendant arms and the two nitrogen atoms of the azobenzene (Figure 1 a), but due to the small bite angle of the azobenzene (N7–U–N8 32.96(9)° in both molecules), this ligand can be considered to occupy a single coordination position. The coordinating atoms describe a distorted bicapped trigonal bipyramid around the uranium centres, with the atoms N3/N3A and the midpoint of the N7–N8/N7A–N8A bond occupying the axial positions (N3–U1–(N7/N8) 173.13(9)° and N3A–U2–(N7A/N8A) 172.41(8)°), the atoms N1/N1A, N2/N2A and N6/N6A located in the equatorial sites and the atoms N5/N5A and N4/N4A capping two of the triangular faces of the bipyramid (Figure 1 b). This coordination geometry is quite different from that of the precursor compound **1**, which has an almost perfect trigonal-prismatic coordination geometry (Figure 1 c and d).^[48]

Relevant bond lengths and angles and a summary of the crystal data and refinement parameters are given in Table 1 and Table S1 (Supporting Information), respectively. The two independent molecules, I and II, in the asymmetric unit feature similar metric parameters and form an enantiomeric pair (Figure S2 in the Supporting Information). The bond lengths observed are consistent with the presence of a U^{IV} centre coordi-

Table 1. Bond lengths [Å] and angles [°] for **2**.

Molecule I		Molecule II	
U1–N1	2.680(3)	U2–N1A	2.726(3)
U1–N2	2.743(3)	U2–N2A	2.753(3)
U1–N3	2.625(3)	U2–N3A	2.645(3)
U1–N4	2.359(2)	U2–N4A	2.374(3)
U1–N5	2.322(3)	U2–N5A	2.334(3)
U1–N6	2.345(3)	U2–N6A	2.337(3)
U1–N7	2.353(3)	U2–N7A	2.357(2)
U1–N8	2.413(3)	U2–N8A	2.400(3)
N7–N8	1.353(4)	N7A–N8	1.350(4)
N7–C31	1.409(4)	N7A–C31A	1.404(4)
N8–C37	1.408(4)	N8A–C37A	1.409(4)
N1–U1–N2	62.23(9)	N1A–U2–N2A	61.71(8)
N1–U1–N3	66.76(9)	N1A–U2–N3A	65.34(8)
N2–U1–N3	68.78(9)	N2A–U2–N3A	67.58(8)
N4–U1–N5	170.57(9)	N4A–U2–N5A	167.04(9)
N4–U1–N6	94.09(9)	N4A–U2–N6A	96.14(9)
N5–U1–N6	88.69(10)	N5A–U2–N6A	92.76(9)
N7–U1–N8	32.96(9)	N7A–U2–N8A	32.96(9)
(N7/N8)–U1–N3 ^[a]	173.13(9)	(N7A/N8A)–U2–N3A ^[a]	172.41(8)

[a] The midpoint between the atoms N7/N8 and N7A/N8A was considered.

ated to a monoanionic azobenzene ligand, and further confirm the evidence provided by the proton NMR spectrum. A clear indication of the radical nature of the azobenzene ligand are the N7–N8/N7A–N8A distances (1.353(4) and 1.350(4) Å in molecules I and II), which have values between those of the N=N bond of azobenzene (1.251 Å)^[69] and the N–N bond of hydrazine (av 1.45 Å).^[70] These bond lengths are within the range of those reported for the related lanthanide complexes [Cp*₂Sm(η²-N₂Ph₂)(THF)] (1.32(1) and 1.39(2) Å),^[52] [(Tp^{Me2})₂Sm(η²-N₂Ph₂)] (1.332(12) Å)^[53] and [Ln(η⁵-C₄Me₂R₂P)₂(η²-N₂Ph₂)] (R = tBu, Ln = Tm; R = SiMe₃, Ln = Sm) (1.351(5) and 1.351(4) Å).^[56] Furthermore, the U–(η²-N₂Ph₂) distances (2.353(3) and 2.413(3) Å in molecule I and 2.357(2) and 2.400(3) Å in molecule II), although slightly shorter, are also comparable to those found in the complex [(SiMe₂NPh)₃-tacn]U^{IV}{η²-(NHC(Me))₂CC≡N]} (2.433(15) and 2.47(2) Å), which bears a bidentate monoanionic N-donor ligand.^[49]

The azobenzene is unsymmetrically bound to the metal centre, with U–N8/N8A distances 0.060 and 0.043 Å longer than the U–N7/N7A distances, as observed in analogous lanthanide complexes.^[52,57,58] However, at variance with lanthanide systems, this dissymmetry is not reflected in the bond lengths between the nitrogen atoms and the *ipso*-carbon atoms of the phenyl rings, which have similar values (1.409(4) and 1.408(4) Å for molecule I and 1.404(4) and 1.409(4) Å for molecule II). The phenyl rings of the azobenzene maintain the same relative orientation as in free *cis*-azobenzene^[69] with slightly less acute dihedral angles (70.37 and 72.15° versus 64.26°), but are significantly more twisted around the N–C_{*ipso*} bonds, as attested by the C_{*ipso*}-N–N–C_{*ipso*} torsion angles, which increase from 8° in free azobenzene to 40° in **2**. Torsion angles of this magnitude would not be possible in the presence of a double bond between the nitrogen atoms and clearly indicate reduction of the N=N bond. Comparable torsion angles were found for

[Cp*₂Sm(η²-N₂Ph₂)(THF)] (44 and 36°),^[52] [(Tp^{Me2})₂Sm(η²-N₂Ph₂)] (46)^[53] and [Ln(η⁵-C₄Me₂R₂P)₂(η²-N₂Ph₂)] (41 and 39°).^[56]

The U–N(amido) and U–N(amine) bond lengths range from 2.322(3) to 2.374(2) Å and 2.625(3) to 2.753(3) Å, respectively. These values are in agreement with those reported for the other tetravalent uranium complexes in this family.^[48,49,51] Compared to the heptacoordinate uranium(III) complex [U{(SiMe₂NPh)₃-tacn}OPPh₃],^[49] which has distances of 2.436(2)–2.468(3) and 2.750(3)–2.785(3) Å for U–N(amido) and U–N(amine) bonds, respectively, the distances found for **2**, in particular those involving the amido nitrogen atoms, are significantly shorter, which reflects the difference in ionic radii of U^{III} and U^{IV}.

The ¹H NMR spectrum of **2**, recorded in [D₆]benzene solution at room temperature, exhibits six broad proton resonances between 22 and –41 ppm for the {(SiMe₂NPh)₃-tacn} ligand (Figure 2). The eighteen protons of the three SiMe₂ groups

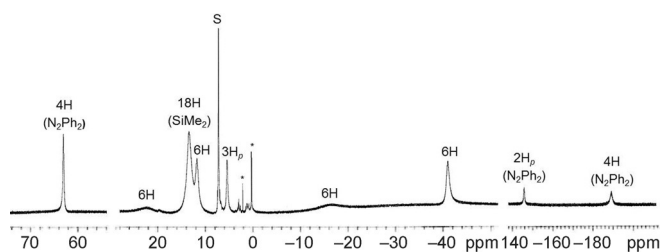


Figure 2. ¹H NMR spectrum (300 MHz) of **2** in [D₆]benzene at room temperature.

give rise to a single peak at low field, the twelve methylene protons of the azamacrocyclic ring to two peaks and the fifteen protons of the aromatic rings to three peaks. This pattern suggests that a fluxional process occurs in solution on the NMR timescale. The most important feature of this spectrum is the position of the resonances assigned to the *ortho*-, *meta*- and *para*-protons of the two phenyl rings of the azobenzene, which appear as three strongly shifted signals at low field (61.94 ppm) and high field (–146.7 and –189.9 ppm). Chemical shifts of this magnitude are strong evidence for the presence of a coordinated radical ligand and have consistently been observed in lanthanide compounds bearing a {N₂Ph₂[•]} radical^[53,55] and in uranium species containing radical ligands.^[71–74]

Low-temperature NMR studies were performed on a [D₈]toluene solution of compound **2**. Gradual cooling of the sample resulted in the progressive shifting and broadening of the proton resonances, indicating slowing of the dynamic process observed at room temperature. At –40 °C all the proton NMR shifts were coalesced in the baseline, but by –60 °C the resonances started to emerge again. At –80 °C, very broad peaks assigned to the {(SiMe₂NPh)₃-tacn} ligand were observed (Figure 3). At this temperature, the ¹H NMR spectrum shows three signals for the SiMe₂ protons, six signals for the CH₂ protons of the tacn fragment and three more signals that could be ascribed to the aromatic protons of the NPh groups. The number of resonances for the methyl protons and the macrocyclic amine indicates that the molecule has *pseudo*-C₃ symme-

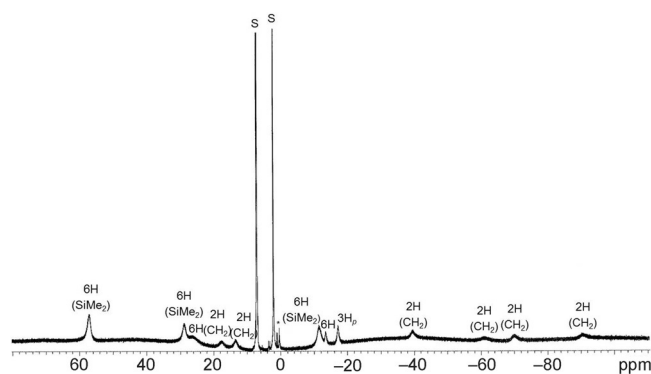


Figure 3. ¹H NMR spectrum (300 MHz) of **2** in [D₈]toluene at –80 °C.

try in solution. The existence of only three peaks for the phenylamido groups shows that the fluxional process that makes the protons of these three groups equivalent is still fast at this temperature on the NMR timescale. This fluxional process could be related to changes in the relative position of the phenylamido groups in the coordination sphere around uranium. Considering that the geometry in solution approaches that found in the solid state (see Figure 1 and discussion above), this process would correspond to the exchange of the nitrogen atoms N₄, N₅ and N₆ between equatorial and capping sites, while maintaining the phenyl groups in the symmetry plane. A similar low-temperature spectrum was found for the iodide derivative [U^{IV}{(SiMe₂NPh)₃-tacn}I].^[48]

Magnetic properties

Measurements of the temperature-dependent magnetic susceptibility of **1** and **2** in the range 3–300 K in a static field of 1000 Oe (Figure 4) revealed paramagnetic behaviour for both compounds.

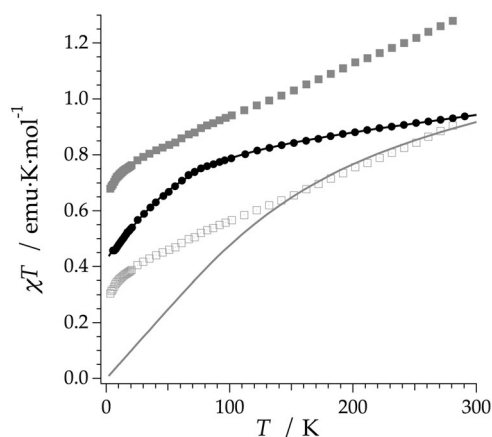


Figure 4. Experimental (symbols) and calculated (lines) temperature dependence of the magnetic susceptibility as χT product for **1** (black circles) and **2** (grey squares) from 2 to 300 K. The solid grey line is the calculated χT product for **2** obtained by using the full single-ion Hamiltonian with the CONDON package (see text). The behaviour of **2** without the radical contribution (assumed to be 0.375 emu K mol^{–1}) is shown as open squares.

For **1** the χT product of $0.94 \text{ emu K mol}^{-1}$ at room temperature is lower than the reported value for the free $5f^3 \text{ U}^{3+}$ ion but within the range of observed values for U^{III} compounds.^[75] For compound **2** χT is higher than in **1** in the entire range of temperature and drops monotonically from $1.32 \text{ emu K mol}^{-1}$ at 300 K to $0.68 \text{ emu K mol}^{-1}$ at 3 K. At 300 K, the χT value is lower than the expected free-ion value for the $5f^2 \text{ U}^{\text{IV}}$ ion of $1.60 \text{ emu K mol}^{-1}$, but slightly higher than the average values ($0.78\text{--}1.19 \text{ emu K mol}^{-1}$) found in most U^{IV} compounds.^[75,76] This is certainly due to the additional contribution of the extra spin from the azobenzene radical. A similar increase in magnetic moment due to the radical-ligand contribution was already observed in the U^{III} complex $[\text{U}(\text{Tp}^{\text{Me}_2})_2(\text{bipy})]$.^[35] At 3 K, a magnetization of $2.33 \mu_B$ was measured. Such a significantly high value at low temperatures is not unusual, and is found in charge-separated uranium(IV) species with radical anion ligands.^[77,78] High magnetic moments at low temperatures were also found in trigonal-bipyramidal uranium(IV) compounds $[\text{Li}(\text{dme})_3][\text{U}(\text{CH}_2\text{SiMe}_3)_5]$ and $[\text{Li}(\text{thf})_4][\text{U}(\text{CH}_2\text{tBu})_5]$ due to changes in the crystal-field splitting patterns.^[79]

The field dependence of the magnetization of **1** (Supporting Information, Figure S5) and **2** (Figure S6) was measured in fields up to 5 T with a SQUID magnetometer at several temperatures down to 0.3 K (sweep rate of 20 Oe s^{-1}) and in fields up to 10 T with a MagLab 2000 system (Oxford Instruments) at temperatures down to 1.7 K (sweep rate of 90 Oe s^{-1}). For **1** no hysteresis was observed down to 1.7 K even at a sweep rate of 90 Oe s^{-1} .

For compound **2**, opening of the hysteresis loop could be clearly observed at 1.7 K, and a butterfly shape emerged, albeit without zero-field coercivity, as typically observed in other mononuclear uranium(III)^[30,33] and uranium(V)^[39] complexes with SMM behaviour (inset of Figure S6 in the Supporting Information). This hysteresis becomes more evident at even lower temperatures (Figure 5). The absence of coercivity is probably due to efficient quantum tunnelling of the magnetization at zero field caused by low-symmetry components of the crystal field. Despite this, at 0.33 K the onset of a plateau

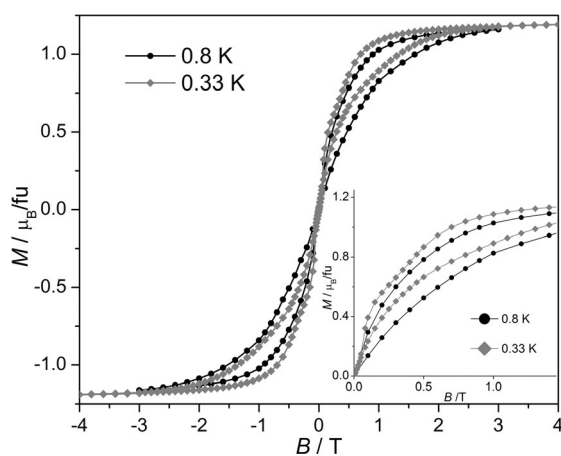


Figure 5. Field dependence of the magnetization for **2** at 0.8 (black circles) and 0.33 K (grey diamonds). The inset shows the details of the curve up to 1.5 T.

at half-value of the magnetization between 0.15 and 0.5 T is observable. Clearer evidence for this intermediate magnetization state would require a complementary study of magnetization under different magnetic-field sweep rates and at even lower temperatures.

An effective-charge electrostatic model can be used to understand the magnetic behaviour of both compounds. In a first step the radial effective charge (REC) model^[80] was applied to the idealized structure (C_{3v}) of **1** by introducing the coordinates of the donor atoms into the SIMPRE computational package.^[81] As these ligands have not been parameterized before, for an initial guess of crystal-field parameters (CFPs), the radial displacement parameter D_r of the REC model^[80] was calculated by using Equation (1):^[82]

$$D_r \approx \left(\frac{N_L}{V_M} \right) \frac{1}{E_M(E_L - E_M)} \quad (1)$$

in which N_L is the coordination number of the complex, V_M the valence of the metal ion, and E_M and E_L are the Pauling electronegativities of the metal and donor atoms, respectively. Such relation was obtained by fitting the phenomenological CFPs of the families $\text{Cs}_2\text{NaYCl}_6:\text{Ln}^{3+}$ and $\text{Cs}_2\text{NaYF}_6:\text{Ln}^{3+}$, $\text{LiYF}_4:\text{Ln}^{3+}$ and $\text{LaCl}_3:\text{Ln}^{3+}$ by means of the crystal structures and the REC model.^[82] Subsequently, the effective charge of the donor atoms was calculated by assuming a similar relation $Z_{\text{eff}} D_r$ to that observed between the REC parameters of different nitrogen-coordinated compounds studied by this model.^[21,80,83,84]

This strategy allowed us to obtain a set of starting CFPs for fitting the temperature-dependent susceptibility of **1** using a full-model approach. As Kögerler et al. recently pointed out, the challenge in modelling actinide complexes is derived from the fact that interelectronic repulsion ($\approx 10^4 \text{ cm}^{-1}$), spin-orbit coupling ($\approx 10^3 \text{ cm}^{-1}$) and ligand-field potential ($\approx 10^3 \text{ cm}^{-1}$) are roughly of the same order of magnitude.^[85] Thus, we introduced this initial trial of calculated CFPs in the package CONDON,^[86] which is suitable to model these systems due to the numerical approach that takes into account all the energetic effects of the free ion and the ligand field. The temperature-dependent magnetic susceptibility data were fitted using the full single-ion Hamiltonian approach with the assumptions: $\zeta_{5f} = 1516 \text{ cm}^{-1}$, $F^2 = 36130 \text{ cm}^{-1}$, $F^4 = 26000 \text{ cm}^{-1}$, $F^6 = 21000 \text{ cm}^{-1}$ ^[87] and C_{3v} ligand-field symmetry. This symmetry approximation implies that the only non-vanishing ligand-field parameters are B_{20} , B_{40} , B_{43} , B_{60} , B_{63} and B_{66} . The least-squares fit (SQ = 0.31 %) yielded $B_{20} = -4900$, $B_{40} = 1788$, $B_{43} = 2144$, $B_{60} = 4363$, $B_{63} = -7055$ and $B_{66} = 8166 \text{ cm}^{-1}$.

The overall ligand-field splitting of the ground multiplet $J = 9/2$ is about 1800 cm^{-1} . This highest state of the ground multiplet is separated from the lowest state of the following first excited multiplet $J = 11/2$, which is located at 3550 cm^{-1} , by only 1750 cm^{-1} . This evidences the need to use a full approach instead of an effective one (assuming Russell-Saunders coupling) for a proper description of the system. All 182 doublets covered by the application of the full basis span an energy interval of about 65970 cm^{-1} . The ground doublet is mainly composed of $M_J = 42\% | \pm 5/2 \rangle + 36\% | \pm 1/2 \rangle + 22\% | \pm 7/2 \rangle$

$2 >$ states. The presence of an important contribution of $\pm 1/2$ in the ground doublet explains the inability of **1** to display SMM behaviour. This is also indicated by the crystallographic structure of the compound, in which the three nitrogen atoms of the SiMe_2NPh group are located 77° on average from the polar coordinate in θ , that is, complex **1** illustrates a situation in which the electron density is distributed near the xy plane. Since U^{III} is an oblate ion with the f -electron density equatorially distributed, the repulsive contacts between ligand and f -electron charge cloud do not favour stabilization of a high M_J value in the ground doublet. Compound **1** evidences that specific symmetries or ligand surroundings may have crucial effects on the magnetic properties of uranium complexes.

Regarding the simulation of the magnetic properties, the fitted χT product and the magnetizations predicted by using the full single-ion Hamiltonian in the CONDON computational package (Figure 4, solid black line) are in excellent agreement with experimental data. The magnetization predicted by this model at 2 K (Supporting Information, Figure S5) is essentially exact at low field/temperature ratios ($H/T < 1 \text{ TK}^{-1}$). There are some deviations at higher fields or lower temperatures, in which the predicted magnetization is above the experimental data, which can be related to small dipolar interactions between the U^{III} centres, which are separated by a distance of about 8.4 \AA , becoming relevant at lower temperatures. In the case of the U^{IV} compound, the larger distance between the magnetic centres ($\approx 10.4 \text{ \AA}$) diminishes the intensity of such interactions.

In a second step, the REC model was used again to obtain an estimation of D_i and Z_i of the groups tacn ($D_i = 1.52 \text{ \AA}$ and $Z_i = 0.04$) and SiMe_2NPh ($D_i = 0.18 \text{ \AA}$ and $Z_i = 2.64$) by direct fitting of the phenomenological CFPs determined by CONDON by using the idealized structure. These results, combined with an analogous study with pyrazolyl ligands in $[\text{U}^{\text{III}}\text{Tp}_3]$ ($D_i = 1.48 \text{ \AA}$ and $Z_i = 0.023$),^[21] allowed us to obtain an estimation of the CFPs of compound **2**. To this end, we introduced the crystal structure of compound **2** in the SIMPRE package, corrected by the determined D_i values, just to obtain a set of CFPs.

Finally, we used CONDON again to calculate the spectroscopic and magnetic properties arising from these CFPs after diagonalizing the full single-ion Hamiltonian. In this case, the presence of a radical and the lack of symmetry elements in the coordination environment limit the usual strategy of a direct fitting of the data. This is especially due to the overparametrization that arises from the geometry of the system. In this sense, combining first-principles calculations with model Hamiltonians to determine the exchange interaction between the f and p spins is a reasonable mid-term goal for the study of this system. Nevertheless, the CFPs predicted by using the REC model and the subsequent diagonalization employing the full single-ion Hamiltonian allow a reasonable prediction of the χT curve (Figure 4, solid grey line).

The agreement at high temperatures is remarkable, considering that the whole theoretical analysis up to this point has been done in the absence of any experimental magnetic data for **2** and is thus a structurally guided, effective-charge, electrostatic prediction. Assuming that this theoretical calculation is

essentially correct for the U^{IV} ion, the observed deviation from experimental data, which starts below 150 K, can be understood as a ferromagnetic exchange coupling between the spin of the radical and the moment of the U^{IV} ion, according to this rough estimation. This coupling is not unexpected, since the orbitals of the radical and uranium ion show a strong interaction. Actinide $5f$ orbitals are considerably more diffuse than lanthanide $4f$ orbitals and form a stronger interaction. Moreover, since the $6d$ orbitals of uranium are energetically in close proximity to the $5f$ orbitals, hybridization of the $5f$ and $6d$ orbitals is potentially possible.

The analysis of the orientations of the $5f/6d$ and p orbitals that would be necessary to fully explain this postulated ferromagnetic exchange is well beyond the scope of this work. The end result is that the experimental χT product at the low temperature limit is on the order of $0.7 \text{ emu K mol}^{-1}$, whereas the calculated value for the U^{IV} ion in the absence of the radical would be practically zero. The calculations were performed with the full single-ion Hamiltonian approach with the default values stored in the CONDON package for U^{IV} :^[88] $\zeta_{5f} = 1926 \text{ cm}^{-1}$, $F^2 = 76557 \text{ cm}^{-1}$, $F^4 = 50078 \text{ cm}^{-1}$, $F^6 = 36429 \text{ cm}^{-1}$ and C_s ligand field. The energy-level scheme of the ground multiplet for U^{IV} in compound **2** is shown in Figure 6. Accord-

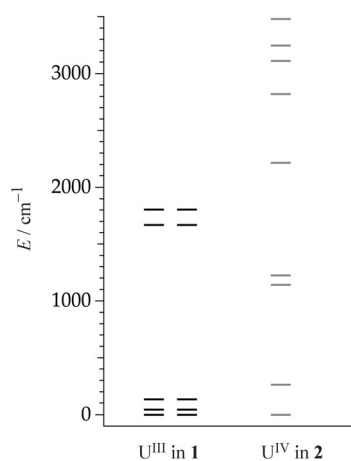


Figure 6. Energy-level scheme of the ground multiplet for the magnetic metal ion in compounds **1** and **2**.

ing to our calculations, the ground state shows an important contribution of $M_J = \pm 4$ (74%) but also the presence of $M_J = 0$ (17%) on the easy axis. Thus, the interaction with the radical seems to play a key role in the slow relaxation of the magnetization in complex **2**, whereas the mere presence of this axial ligand would not be enough. In other words, an equivalent ligand field produced by a diamagnetic but otherwise similar coordination sphere would produce a magnetic behaviour similar to that of **1**.

Regarding the radical contribution, the main effect of the extra electron spin is to switch the parity from non-Kramers to Kramers. A moderate magnetic exchange suffices to alter the quantum-mechanical character of the ground-state doublet. Thus, from a tunnel-split doublet that is mainly a mixture of

$M_J = +4$, $M_J = -4$ and $M_J = 0$ one expects to obtain two doublets that are dominated by $M_J = \pm 9/2$ and $M_J = \pm 7/2$, respectively. Solving a complete model considering the U^{IV} ion, including its excited states, together with the radical, was impractical at this point. Nevertheless, a simplified model consisting of an anisotropic effective $S = 1$ (non-Kramers) state exchange-coupled with an $S = 1/2$ state suffices to evidence this effect (see details in the Supporting Information). From the point of view of the radical, the coupling to the anisotropic magnetic momentum produces an extremely anisotropic radical. However, **2** was found to be EPR silent. Further information on the magnetization dynamics was obtained by ac susceptibility measurements at low temperatures (1.6–10 K), with an ac field of 5 Oe in the frequency range 10 Hz to 10 kHz and in several static dc fields. For **1** no evidence for slow magnetic relaxation was observed with both the in-phase (χ') and out-of-phase (χ'') components of susceptibility being frequency-independent, even in different static magnetic fields. This is not the situation for **2**, which at zero field exhibits χ' and χ'' components that are frequency-independent (Supporting Information, Figure S7) but starts to show a strong frequency dependence upon the application of a small static (dc) field. By studying the ac susceptibility in different applied static magnetic fields the longest relaxation time was observed to occur to 1000 Oe (Supporting Information, Figure S8). With temperature variation a well-resolved local maximum appears in χ'' , which shifts to higher temperatures as the frequency increases, as shown in Figure 7b. Above 1000 Oe the magnetic field only slightly enhances the frequency and temperature dependence of the peaks, with χ' showing broad maxima (Figure 7c), and

the maxima of χ'' becoming better resolved for low frequencies (Figure 7d) with no significant increase in the magnitude of the peaks (see also Supporting Information, Figure S9).

At fixed temperatures between 1.6 and 6 K, the frequency dependence of the ac susceptibility also shows slow magnetic relaxation under applied static dc fields, (Figure 8a and b and S10, S11 and S12 in the Supporting Information) clearly denoting SMM behaviour with reduction of the quantum tunnelling of magnetization through spin-reversal barrier via degenerate $\pm M_J$ levels. From the $\chi(\omega)$ data for three different static fields, semi-circular Cole–Cole diagrams were obtained in the temperature range 1.6–6 K (Figure 8c and Supporting Information, Figures S10–S12), and fitting to the generalized Debye model^[89] afforded α values of less than 0.1 (see Tables S2–S4 in the Supporting Information), which support the existence of a single relaxation process.

Magnetization relaxation times could also be extracted by considering that compound **2** relaxes by a thermally activated Orbach process. As seen in Figure 9a the Arrhenius law fits, calculated by using the equation $\tau = \tau_0 \exp(U/k_B T)$, in which U is the effective energy barrier and k_B the Boltzmann constant, yielded barriers of $U = 14.1$, 16.9 and 17.6 K at 1000, 2000 and 2500 Oe, respectively, on the same order of magnitude as those observed for mononuclear U^{III} complexes.^[16, 18, 31, 33, 35] Below 3.5 K it approached a temperature-independent regime of the relaxation time that is similar for all different static fields. This linear relationship of $\ln(1/\tau)$ with $1/T$, indicative of an Orbach process, does not cover the whole range of temperature-dependent data. Thus, to find some other contributions to the relaxation pathway a Raman process was also fitted to

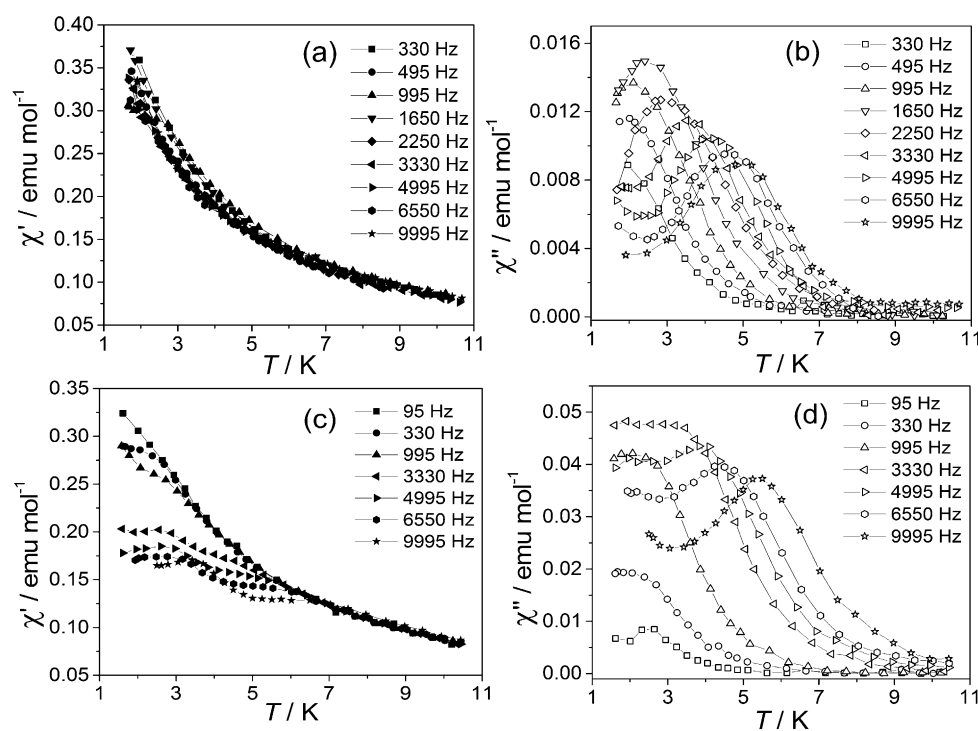


Figure 7. In-phase χ' and out-of-phase χ'' components of ac susceptibility at different frequencies from 1.7 to 10 K for **2** at $H_{ac} = 5$ Oe and $H_{dc} = 1000$ Oe (a, b), and 2500 Oe (c, d). See also Figure S9 of the Supporting Information.

these experimental data under the assumption $1/\sqrt{\tau} = a + bT$, that is, a linear slope in $1/\sqrt{\tau}$ versus T . These results can be seen in Figure 9b, in which the coefficients $a = 2.2$, 2.22 and 2.17 and $b = 0.21$, 0.23 and 0.25 were obtained for static fields of 1000, 2000 and 2500 Oe, respectively. By comparison to the Orbach process, these fits clearly show that the Raman process covers a wider range of temperatures, in particular at 1000 Oe, for which only below 2 K does an independent temperature regime occur through the dominance of quantum tunnelling effects.

Conclusions

We have prepared and characterized a new mononuclear U^{IV} complex with a radical azobenzene ligand, namely, $[(SiMe_2NPh)_3-tacn]U^{IV}(\eta^2-N_2Ph_2)$ (**2**).

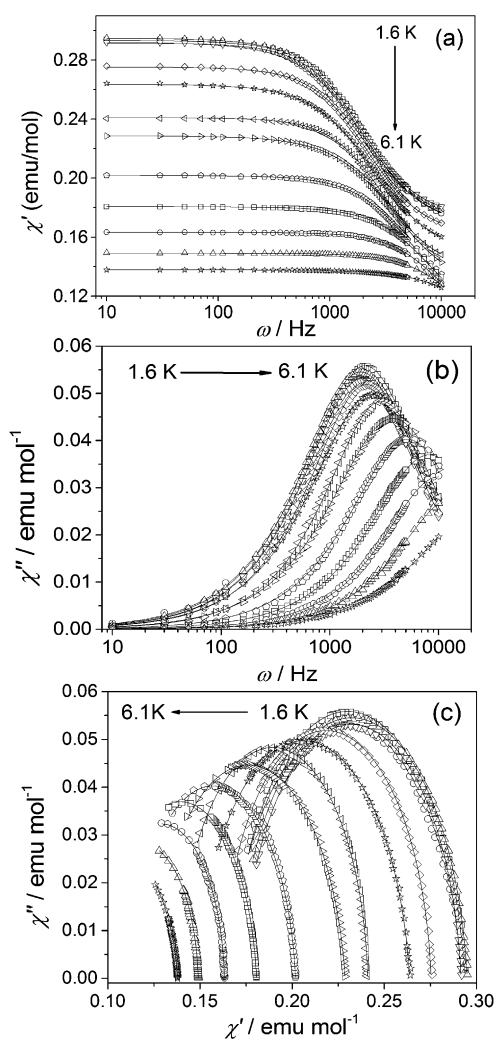


Figure 8. a) In-phase and b) out-of-phase components of ac susceptibility at different frequencies in the 1.7 to 10 K temperature range for **2** at $H_{ac} = 5$ Oe and $H_{dc} = 2500$ Oe. c) Cole–Cole plots with best fits to the Debye model (see also Figures S10–S12 of the Supporting Information).

The magnetic properties of **2** and its precursor $[U^{III}\{(SiMe_2NPh)_3-tacn\}]$ (**1**) were studied by static magnetization and ac susceptibility measurements. At variance with several trivalent uranium compounds recently studied, the magnetic properties of **1** do not show a clear sign of slow relaxation of the magnetization down to 1.7 K, and this evidences the crucial role of the coordination environment. In contrast, compound **2** shows at low temperatures a clear indication of slow relaxation of the magnetization in applied static dc fields in the range 1–2.5 kOe, a large hysteresis in the magnetization curves and is thus the first uranium(IV) compound with SMM behaviour.

The relaxation barrier associated with the thermally activated regime of the relaxation, 17.6 K at 2500 Oe, is on the same order of magnitude as those observed for mononuclear U^{III} complexes with SMM behaviour. This unprecedented behaviour for uranium(IV) seems to result from the interaction of the metal ion with the paramagnetic ligand, which switches the parity from non-Kramers to Kramers. This may provide a new

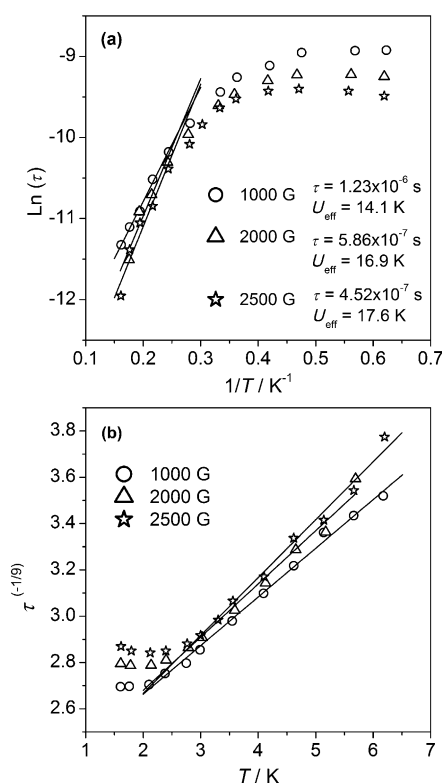


Figure 9. a) Plot of $\ln \tau$ versus T^{-1} with fits to the Arrhenius law. b) Plot of 9th root of the relaxation frequency versus temperature with fittings assuming a Raman process. $H_{dc} = 1000$ Oe (circles), $H_{dc} = 2000$ Oe (triangles) and $H_{dc} = 2500$ Oe (stars); $H_{ac} = 5$ Oe.

strategy to design SIMs with non-Kramers ions. When considering the use of this strategy to extend relaxation times in rare earth metal complexes, it is important to consider that tunnelling can only be blocked for temperatures much smaller than the coupling energy. Therefore, to achieve significant success in enhancing the blocking temperature, the exchange coupling to and via the radical must be significant, which is exceptional for lanthanides but more common in actinides.

Experimental Section

General considerations

All manipulations were carried out under a nitrogen atmosphere in a glovebox or by using standard Schlenk and vacuum-line techniques. Toluene and *n*-hexane were predried with 4 Å molecular sieves, freshly distilled from sodium/benzophenone under nitrogen atmosphere and degassed with freeze–pump–thaw cycles. $[D_6]$ benzene and $[D_8]$ toluene were vacuum-distilled from sodium/benzophenone and stored in PTFE-valve glass ampoules under nitrogen. Azobenzene was purchased from Aldrich and dried under vacuum prior to use. $[U\{(SiMe_2NPh)_3-tacn\}]$ (**1**) was prepared according to a previously reported procedure.^[48] 1H NMR spectra were recorded with Varian INOVA-300 and Bruker Avance II 300 spectrometers. Chemical shifts were referenced to resonances of the residual protonated solvents relative to TMS ($[D_6]$ benzene, $\delta = 7.16$ ppm; $[D_8]$ toluene, $\delta = 2.09$ ppm). IR spectra were recorded with Bruker Tensor 27 and Thermo Scientific Nicolet i550 FT-IR spectrometers. UV/Vis/NIR spectra were recorded with a Varian

Cary 5G spectrometer in 1 cm quartz cells. CHN elemental analyses were performed in-house with a EA1110 CE Instruments automatic analyser.

Synthesis of $[(\text{SiMe}_2\text{NPh})_3\text{-tacn}]\text{U}^{\text{IV}}(\eta^2\text{-N}_2\text{Ph}_2)$ (**2**)

A toluene solution of azobenzene (33 mg, 0.18 mmol) was added dropwise to a solution of **1** (145 mg, 0.18 mmol) in the same solvent at room temperature. A colour change from dark brown to dark green was immediately observed. The reaction mixture was left stirring for 2 h. After this time, the solvent was evaporated under reduced pressure to give a dark green solid, which was washed with *n*-hexane and vacuum-dried. Yield: 106 mg (59%); $^1\text{H NMR}$ (300.1 MHz, $[\text{D}_6]$ Benzene, 296 K, TMS): δ = 61.94 (s, 4H, N_2Ph_2), 22 (vbr, 6H), 13.23 (s, 18H, SiMe_2), 11.67 (s, 6H), 5.36 (s, 3H, $\text{H}_p\text{-NPh}$), -17 (vbr, 6H), -40.81 (s, 6H), -146.7 (s, 2H, $\text{H}_p\text{-N}_2\text{Ph}_2$), -189.9 ppm (s, 4H, N_2Ph_2); $^1\text{H NMR}$ (300.1 MHz, $[\text{D}_8]$ toluene, 193 K, TMS): δ = 57.08 (s, 6H, SiMe_2), 28.75 (s, 6H, SiMe_2), 26 (vbr, 6H, NPh), 18.1 (br, 2H, CH_2), 13.1 (br, 2H, CH_2), -11.27 (s, 6H, SiMe_2), -13.18 (s, 6H, NPh), -17.24 (s, 3H, $\text{H}_p\text{-NPh}$), -39.69 (br, 2H, CH_2), -60 (vbr, 2H, CH_2), -69.8 (br, 2H, CH_2), -91 ppm (vbr, 2H, CH_2). No resonances for N_2Ph_2 were observed at this temperature; elemental analysis calcd (%) for $\text{C}_{42}\text{H}_{55}\text{N}_8\text{Si}_3\text{U}$: C 50.74, H 5.58, N 11.27; found: C 49.79, H 5.91, N 11.15.

Single-crystal X-ray diffraction

A single crystal of **2** was selected and coated with Fomblin Y60 LVAC 25/6 oil (Aldrich) in a glovebox and rapidly mounted on a Bruker AXS-KAPPA APEX II CCD area-detector diffractometer equipped with graphite-monochromated $\text{MoK}\alpha$ radiation ($\lambda = 0.71073 \text{ \AA}$). Cell parameters were retrieved by using Bruker SMART S5 software and refined with Bruker SAINT on all observed reflections.^[90] Absorption corrections were applied with SADABS.^[91] The structure was solved by direct methods with SIR97^[92] and refined by full-matrix, least-squares refinement on F^2 with SHELXL-97,^[93] both included in the package of software programs WINGX.^[94] All non-hydrogen atoms were refined with anisotropic thermal motion parameters. All hydrogen atoms were inserted at calculated positions based on the geometries of their attached carbon atoms. The illustration of the molecular structure was made with Mercury 3.3.^[95] CCDC 1054616 contains the supplementary crystallographic data for this paper. These data are provided free of charge by The Cambridge Crystallographic Data Centre.

Magnetic measurements

Two different batches of compounds **1** and **2** were measured as crystalline powder imbedded in *n*-hexane with identical results within experimental uncertainty. Due to their high air sensitivity, the samples were sealed under vacuum inside a quartz tube. Magnetization was measured with a 6.5 T S700X SQUID magnetometer (Cryogenic Ltd.) in the temperature range 2–300 K at several magnetic fields and with a ^3He insert for measurements down to 0.3 K. Additional field-dependent magnetization up to 10 T (and 10 T at 1.7 K) and ac susceptibility measurements were taken with a MagLab 2000 system (Oxford Instruments) at temperatures down to 1.7 K. The paramagnetic data were obtained after correction for the core diamagnetism estimated from Pascal's constants as $\chi_D = -397.3 \times 10^{-6} \text{ emu mol}^{-1}$ and $\chi_D = - \text{emu mol}^{-1}$ for compounds **1** and **2**, respectively.

Acknowledgements

$\text{C}^2\text{TN/IST}$ authors gratefully acknowledge the FCT support through the UID/Multi/04349/2013 project. The experimental support of Joaquim Branco is gratefully acknowledged. J.T.C. and M.A.A. thank FCT (Portugal) for doctoral and post-doctoral grants (SFRH/BD/84628/2012 and SFRH/BPD/74194/2010). This work was partially supported by FCT (Portugal) under contracts PTDC/REQ-SUP/1413/2012 and RECI/REQ-QIN/0189/2012, the EU (ERC Advanced Grant SPINMOL and ERC Consolidator Grant DECRESIM), the Spanish MINECO (grant MAT2011-22785) and the Generalitat Valenciana (Prometeo and ISIC Programmes of excellence). A.G.-A. acknowledges funding by the MINECO (Ramón y Cajal contract). J.J.B. thanks the Spanish MINECO for an FPU predoctoral grant.

Keywords: azo compounds · magnetic properties · N ligands · radicals · uranium

- [1] D. Gatteschi, R. Sessoli, *Angew. Chem. Int. Ed.* **2003**, *42*, 268–297; *Angew. Chem.* **2003**, *115*, 278–309.
- [2] A. Dei, D. Gatteschi, *Angew. Chem. Int. Ed.* **2011**, *50*, 11852–11858; *Angew. Chem.* **2011**, *123*, 12054–12060.
- [3] M. Mannini, F. Pineider, C. Danieli, F. Totti, L. Sorace, P. Sainctavit, M. A. Arrio, E. Otero, L. Joly, J. C. Cezar, A. Cornia, R. Sessoli, *Nature* **2010**, *468*, 417–421.
- [4] D. Gatteschi, R. Sessoli, J. Villain, *Molecular Nanomagnets*, Oxford University Press, Oxford, **2006**.
- [5] R. A. Layfield, *Organometallics* **2014**, *33*, 1084–1099.
- [6] K. S. Pedersen, J. Bendix, R. Clerac, *Chem. Commun.* **2014**, *50*, 4396–4415.
- [7] M. Clemente-León, E. Coronado, C. J. Gómez-García, M. López-Jordà, A. Camón, A. Repollés, F. Luis, *Chem. Eur. J.* **2014**, *20*, 1669–1676.
- [8] J. Luzon, R. Sessoli, *Dalton Trans.* **2012**, *41*, 13556–13567.
- [9] L. Sorace, C. Benelli, D. Gatteschi, *Chem. Soc. Rev.* **2011**, *40*, 3092–3104.
- [10] N. Ishikawa, M. Sugita, T. Ishikawa, S.-y. Koshihara, Y. Kaizu, *J. Am. Chem. Soc.* **2003**, *125*, 8694–8695.
- [11] H. L. C. Feltham, S. Brooker, *Coord. Chem. Rev.* **2014**, *276*, 1–33.
- [12] D. N. Woodruff, R. E. P. Winpenny, R. A. Layfield, *Chem. Rev.* **2013**, *113*, 5110–5148.
- [13] S. Demir, I.-R. Jeon, J. R. Long, T. D. Harris, *Coord. Chem. Rev.* **2015**, *289*–290, 149–176.
- [14] M. A. Aldamen, J. M. Clemente-Juan, E. Coronado, C. Martí-Gastaldo, A. Gaita-Ariño, *J. Am. Chem. Soc.* **2008**, *130*, 8874–8875.
- [15] N. Magnani, *Int. J. Quantum Chem.* **2014**, *114*, 755–759.
- [16] L. C. J. Pereira, C. Camp, J. T. Coutinho, L. Chatelain, P. Maldivi, M. Almeida, M. Mazzanti, *Inorg. Chem.* **2014**, *53*, 11809–11811.
- [17] C. A. P. Goodwin, F. Tuna, E. J. L. McInnes, S. T. Liddle, J. McMaster, I. J. Victoria-Yrezabal, D. P. Mills, *Chem. Eur. J.* **2014**, *20*, 14579–14583.
- [18] K. R. Meihaus, J. R. Long, *Dalton Trans.* **2015**, *44*, 2517–2528.
- [19] G. A. Craig, M. Murrie, *Chem. Soc. Rev.* **2015**, *44*, 2135–2147.
- [20] J. D. Rinehart, J. R. Long, *Chem. Sci.* **2011**, *2*, 2078–2085.
- [21] J. J. Baldovi, S. Cardona-Serra, J. M. Clemente-Juan, E. Coronado, A. Gaita-Ariño, *Chem. Sci.* **2013**, *4*, 938–946.
- [22] R. J. Blagg, L. Ungur, F. Tuna, J. Speak, P. Comar, D. Collison, W. Wernsdorfer, E. J. L. McInnes, L. F. Chibotaru, R. E. P. Winpenny, *Nat. Chem.* **2013**, *5*, 673–678.
- [23] F. Habib, M. Murugesu, *Chem. Soc. Rev.* **2013**, *42*, 3278–3288.
- [24] P. Zhang, L. Zhang, J. Tang, *Dalton Trans.* **2015**, *44*, 3923–3929.
- [25] M. Atanasov, D. Aravena, E. Sutorina, E. Bill, D. Maganas, F. Neese, *Coord. Chem. Rev.* **2015**, *289*–290, 177–214.
- [26] D. P. Mills, F. Moro, J. McMaster, J. van Slageren, W. Lewis, A. J. Blake, S. T. Liddle, *Nat. Chem.* **2011**, *3*, 454–460.
- [27] F. Moro, D. P. Mills, S. T. Liddle, J. van Slageren, *Angew. Chem. Int. Ed.* **2013**, *52*, 3430–3433; *Angew. Chem.* **2013**, *125*, 3514–3517.

- [28] J. D. Rinehart, J. R. Long, *J. Am. Chem. Soc.* **2009**, *131*, 12558–12559.
- [29] J. D. Rinehart, K. R. Meihaus, J. R. Long, *J. Am. Chem. Soc.* **2010**, *132*, 7572–7573.
- [30] K. R. Meihaus, J. D. Rinehart, J. R. Long, *Inorg. Chem.* **2011**, *50*, 8484–8489.
- [31] M. A. Antunes, L. C. J. Pereira, I. C. Santos, M. Mazzanti, J. Marcalo, M. Almeida, *Inorg. Chem.* **2011**, *50*, 9915–9917.
- [32] J. D. Rinehart, J. R. Long, *Dalton Trans.* **2012**, *41*, 13572–13574.
- [33] J. T. Coutinho, M. A. Antunes, L. C. J. Pereira, H. Bolvin, J. Marcalo, M. Mazzanti, M. Almeida, *Dalton Trans.* **2012**, *41*, 13568–13571.
- [34] K. R. Meihaus, S. G. Minasian, W. W. Lukens, S. A. Kozimor, D. K. Shuh, T. Tyliczszak, J. R. Long, *J. Am. Chem. Soc.* **2014**, *136*, 6056–6068.
- [35] J. T. Coutinho, M. A. Antunes, L. C. J. Pereira, J. Marcalo, M. Almeida, *Chem. Commun.* **2014**, *50*, 10262–10264.
- [36] M. A. Antunes, I. C. Santos, H. Bolvin, L. C. J. Pereira, M. Mazzanti, J. Marcalo, M. Almeida, *Dalton Trans.* **2013**, *42*, 8861–8867.
- [37] M. R. MacDonald, M. E. Fieser, J. E. Bates, J. W. Ziller, F. Furche, W. J. Evans, *J. Am. Chem. Soc.* **2013**, *135*, 13310–13313.
- [38] H. S. La Pierre, A. Scheurer, F. W. Heinemann, W. Hieringer, K. Meyer, *Angew. Chem. Int. Ed.* **2014**, *53*, 7158–7162; *Angew. Chem.* **2014**, *126*, 7286–7290.
- [39] D. M. King, F. Tuna, J. McMaster, W. Lewis, A. J. Blake, E. J. L. McInnes, S. T. Liddle, *Angew. Chem. Int. Ed.* **2013**, *52*, 4921–4924; *Angew. Chem.* **2013**, *125*, 5021–5024.
- [40] N. M. Edelstein, G. H. Lander, *The Chemistry of Actinide and Transactinide Elements*, Vol. 4, 3rd ed. (Eds.: L. R. Morss, N. M. Edelstein, J. Fuger), Springer, Dordrecht, **2006**, Chapter 20.
- [41] J. D. Rinehart, B. M. Bartlett, S. A. Kozimor, J. R. Long, *Inorg. Chim. Acta* **2008**, *361*, 3534–3538.
- [42] B. S. Newell, T. C. Schwaab, M. P. Shores, *Inorg. Chem.* **2011**, *50*, 12108–12115.
- [43] S. A. Kozimor, B. M. Bartlett, J. D. Rinehart, J. R. Long, *J. Am. Chem. Soc.* **2007**, *129*, 10672–10674.
- [44] J. J. Le Roy, S. I. Gorelsky, I. Korobkov, M. Murugesu, *Organometallics* **2015**, *34*, 1415–1418.
- [45] J. D. Rinehart, M. Fang, W. J. Evans, J. R. Long, *Nat. Chem.* **2011**, *3*, 538–542.
- [46] J. D. Rinehart, M. Fang, W. J. Evans, J. R. Long, *J. Am. Chem. Soc.* **2011**, *133*, 14236–14239.
- [47] E. Moreno Pineda, N. F. Chilton, R. Marx, M. Dörfel, D. O. Sells, P. Neugebauer, S.-D. Jiang, D. Collison, J. van Slageren, E. J. L. McInnes, R. E. P. Winpenny, *Nat. Commun.* **2014**, *5*, 5243.
- [48] B. Monteiro, D. Roitershtein, H. Ferreira, J. R. Ascenso, A. M. Martins, Â. Domingos, N. Marques, *Inorg. Chem.* **2003**, *42*, 4223–4231.
- [49] M. A. Antunes, M. Dias, B. Monteiro, A. Domingos, I. C. Santos, N. Marques, *Dalton Trans.* **2006**, *27*, 3368–3374.
- [50] M. A. Antunes, PhD Thesis, Universidade de Lisboa, **2006**.
- [51] C. Camp, M. A. Antunes, G. Garcia, I. Ciofini, I. C. Santos, J. Pecaut, M. Almeida, J. Marcalo, M. Mazzanti, *Chem. Sci.* **2014**, *5*, 841–846.
- [52] W. J. Evans, D. K. Drummond, L. R. Chamberlain, R. J. Doedens, S. G. Bott, H. Zhang, J. L. Atwood, *J. Am. Chem. Soc.* **1988**, *110*, 4983–4994.
- [53] J. Takats, X. W. Zhang, V. W. Day, T. A. Eberspacher, *Organometallics* **1993**, *12*, 4286–4288.
- [54] W. J. Evans, K. J. Forrestal, J. W. Ziller, *J. Am. Chem. Soc.* **1998**, *120*, 9273–9282.
- [55] D. J. Berg, J. M. Boncella, R. A. Andersen, *Organometallics* **2002**, *21*, 4622–4631.
- [56] D. Turcitu, F. Nief, L. Ricard, *Chem. Eur. J.* **2003**, *9*, 4916–4923.
- [57] W. J. Evans, T. M. Champagne, J. W. Ziller, *Organometallics* **2007**, *26*, 1204–1211.
- [58] J. Andrez, J. Pécaut, P.-A. Bayle, M. Mazzanti, *Angew. Chem. Int. Ed.* **2014**, *53*, 10448–10452; *Angew. Chem.* **2014**, *126*, 10616–10620.
- [59] W. J. Evans, D. K. Drummond, S. G. Bott, J. L. Atwood, *Organometallics* **1986**, *5*, 2389–2391.
- [60] E. D. Brady, D. L. Clark, D. W. Keogh, B. L. Scott, J. G. Watkin, *J. Am. Chem. Soc.* **2002**, *124*, 7007–7015.
- [61] W. J. Evans, S. A. Kozimor, J. W. Ziller, *Chem. Commun.* **2005**, *37*, 4681–4683.
- [62] W. J. Evans, K. A. Miller, S. A. Kozimor, J. W. Ziller, A. G. DiPasquale, A. L. Rheingold, *Organometallics* **2007**, *26*, 3568–3576.
- [63] W. J. Evans, E. Montalvo, S. A. Kozimor, K. A. Miller, *J. Am. Chem. Soc.* **2008**, *130*, 12258–12259.
- [64] D. P. Cladis, J. J. Kiernicki, P. E. Fanwick, S. C. Bart, *Chem. Commun.* **2013**, *49*, 4169–4171.
- [65] B. P. Warner, B. L. Scott, C. J. Burns, *Angew. Chem. Int. Ed.* **1998**, *37*, 959–960; *Angew. Chem.* **1998**, *110*, 1005–1007.
- [66] R. G. Peters, B. P. Warner, C. J. Burns, *J. Am. Chem. Soc.* **1999**, *121*, 5585–5586.
- [67] P. L. Diaconescu, P. L. Arnold, T. A. Baker, D. J. Mindiola, C. C. Cummins, *J. Am. Chem. Soc.* **2000**, *122*, 6108–6109.
- [68] P. L. Diaconescu, C. C. Cummins, *Inorg. Chem.* **2012**, *51*, 2902–2916.
- [69] A. Mostad, C. Romming, *Acta Chem. Sc.* **1971**, *25*, 3561–3568.
- [70] Cambridge Structural Data Base.
- [71] T. Mehdoui, J.-C. Berthet, P. Thuéry, L. Salmon, E. Rivière, M. Ephritikhine, *Chem. Eur. J.* **2005**, *11*, 6994–7006.
- [72] S. J. Kraft, P. E. Fanwick, S. C. Bart, *Inorg. Chem.* **2010**, *49*, 1103–1110.
- [73] J. J. Kiernicki, B. S. Newell, E. M. Matson, N. H. Anderson, P. E. Fanwick, M. P. Shores, S. C. Bart, *Inorg. Chem.* **2014**, *53*, 3730–3741.
- [74] E. M. Matson, J. J. Kiernicki, N. H. Anderson, P. E. Fanwick, S. C. Bart, *Dalton Trans.* **2014**, *43*, 17885–17888.
- [75] D. R. Kindra, W. J. Evans, *Chem. Rev.* **2014**, *114*, 8865–8882.
- [76] S. J. Kraft, U. J. Williams, S. R. Daly, E. J. Schelter, S. A. Kozimor, K. S. Boland, J. M. Kikkawa, W. P. Forrest, C. N. Christensen, D. E. Schwarz, P. E. Fanwick, D. L. Clark, S. D. Conradson, S. C. Bart, *Inorg. Chem.* **2011**, *50*, 9838–9848.
- [77] E. M. Matson, S. M. Franke, N. H. Anderson, T. D. Cook, P. E. Fanwick, S. C. Bart, *Organometallics* **2014**, *33*, 1964–1971.
- [78] O. P. Lam, P. L. Feng, F. W. Heinemann, J. M. O'Connor, K. Meyer, *J. Am. Chem. Soc.* **2008**, *130*, 2806–2816.
- [79] S. Fortier, B. C. Melot, G. Wu, T. W. Hayton, *J. Am. Chem. Soc.* **2009**, *131*, 15512–15521.
- [80] J. J. Baldoví, J. J. Borrás-Almenar, J. M. Clemente-Juan, E. Coronado, A. Gaita-Ariño, *Dalton Trans.* **2012**, *41*, 13705–13710.
- [81] J. J. Baldoví, S. Cardona-Serra, J. M. Clemente-Juan, E. Coronado, A. Gaita-Ariño, A. Palií, *J. Comput. Chem.* **2013**, *34*, 1961–1967.
- [82] J. J. Baldoví, A. Gaita-Ariño, E. Coronado, *Dalton Trans.* **2015**, *44*, 12535–12538.
- [83] K. Qian, J. J. Baldoví, S. D. Jiang, A. Gaita-Ariño, Y.-Q. Zhang, J. Overgaard, B.-W. Wang, E. Coronado, S. Gao, *Chem. Sci.* **2015**, *6*, 4587–4593.
- [84] J. J. Baldoví, J. M. Clemente-Juan, E. Coronado, A. Gaita-Ariño, *Polyhedron* **2013**, *66*, 39–42.
- [85] J. van Leusen, M. Speldrich, H. Schilder, P. Kögerler, *Coord. Chem. Rev.* **2015**, *289–290*, 137–148.
- [86] M. Speldrich, H. Schilder, H. Lueken, P. Kögerler, *Isr. J. Chem.* **2011**, *51*, 215–227.
- [87] C. Apostolidis, A. Morgenstern, J. Rebizant, B. Kanellakopulos, O. Walter, B. Powietzka, M. Karbowiak, H. Reddmann, H. D. Amberger, *Z. Anorg. Allg. Chem.* **2010**, *636*, 201–208.
- [88] J. P. Delaux, A. J. Freeman, in *Handbook on the Physics and Chemistry of the Actinides Vol. 1* (Ed.: A. J. Freeman, G. H. Lander), Elsevier, Amsterdam, **1984**, Chapter 1, pp. 18, 51, 66, and 118.
- [89] K. S. Cole, R. H. Cole, *J. Chem. Phys.* **1941**, *9*, 341–351.
- [90] Bruker, SMART and SAINT, Bruker AXS Inc., Madison, Wisconsin, USA, **2004**.
- [91] G. M. Sheldrick, SADABS, Bruker AXS Inc., Madison, Wisconsin, USA, **2004**.
- [92] A. Altomare, M. C. Burla, M. Camalli, G. L. Cascarano, C. Giacovazzo, A. Guagliardi, A. G. G. Moliterni, G. Polidori, R. Spagna, *J. Appl. Crystallogr.* **1999**, *32*, 115–119.
- [93] G. M. Sheldrick, SHELXL-97, Program for the Refinement of Crystal Structure, University of Gottingen, Germany, **1997**.
- [94] J. L. Farrugia, *J. Appl. Crystallogr.* **1999**, *32*, 837–838.
- [95] C. F. Macrae, P. R. Edgington, P. McCabe, E. Pidcock, G. P. Shields, R. Taylor, M.; Towler, J. van De Streek, *J. Appl. Crystallogr.* **2006**, *39*, 453–457; Towler, J. van De Streek, *J. Appl. Crystallogr.* **2006**, *39*, 453–457.

Received: August 8, 2015

Revised: September 24, 2015

Published online on November 5, 2015